J Physiol (2003), **553.3**, *pp.* 775–788
DOI: 10.1113/jphysiol.2003.054247

www.jphysiol.org

Buffer kinetics shape the spatiotemporal patterns of IP_3-evoked Ca^{2+} signals

Sheila L. Dargan and Ian Parker

Department of Neurobiology and Behavior, University of California Irvine, CA 92697-4550, USA

Ca^{2+} liberation through inositol 1,4,5-trisphosphate receptors (IP_3Rs) plays a universal role in cell regulation, and specificity of cell signalling is achieved through the spatiotemporal patterning of Ca^{2+} signals. IP_3Rs display Ca^{2+}-induced Ca^{2+} release (CICR), but are grouped in clusters so that regenerative Ca^{2+} signals may remain localized to individual clusters, or propagate globally between clusters by successive cycles of Ca^{2+} diffusion and CICR. We used confocal microscopy and photoreleased IP_3 in *Xenopus* oocytes to study how these properties are modulated by mobile cytosolic Ca^{2+} buffers. EGTA (a buffer with slow 'on-rate') speeded Ca^{2+} signals and 'balkanized' Ca^{2+} waves by dissociating them into local signals. In contrast, BAPTA (a fast buffer with similar affinity) slowed Ca^{2+} responses and promoted 'globalization' of spatially uniform Ca^{2+} signals. These actions are likely to arise through differential effects on Ca^{2+} feedback within and between IP_3R clusters, because Ca^{2+} signals evoked by influx through voltage-gated channels were little affected. We propose that cell-specific expression of Ca^{2+}-binding proteins with distinct kinetics may shape the time course and spatial distribution of IP_3-evoked Ca^{2+} signals for specific physiological roles.

(Received 30 August 2003; accepted after revision 7 October 2003; first published online 10 October 2003)
Corresponding author S. L. Dargan: Department of Neurobiology and Behavior, University of California Irvine, CA 92697-4550, USA. Email: sdargan@uci.edu

Cytosolic Ca^{2+} ions regulate numerous aspects of cellular activity in virtually all cell types (Berridge *et al.* 2000). This versatility is made possible by the diverse mechanisms by which Ca^{2+} signals are generated and transmitted to act over very different time and distance scales (Berridge *et al.* 2000; Marchant & Parker, 2000). Endogenous Ca^{2+} binding proteins play a key role in determining the magnitude, kinetics and spatial distribution of cytosolic Ca^{2+} signals, and typically buffer most (> 90 %) of the total Ca^{2+} ions in the cytosol (Berridge *et al.* 2000). As well as simply reducing the availability of free cytosolic Ca^{2+} ions, buffers also affect their diffusional mobility. Immobile buffers reduce the effective diffusion coefficient for Ca^{2+}, whereas mobile buffers can act as a 'shuttle' to speed Ca^{2+} diffusion in the presence of immobile buffers (Stern, 1992; Roberts, 1994). It is thus likely that cells utilize buffers to shape Ca^{2+} signals for their specific functions; a notion supported by observations that different cell types – particularly sub-populations of neurons – selectively express mobile Ca^{2+} binding proteins (e.g. parvalbumin and calretinin) with differing properties (Andressen *et al.* 1993). However, the functional consequences of selective buffer expression remain unclear (Neher, 2000; Schwaller *et al.* 2002).

Most experimental and theoretical investigations of cellular Ca^{2+} buffers have concentrated on signals arising from a fixed 'pulse' of Ca^{2+}, e.g. Ca^{2+} entry through voltage- or ligand-gated membrane channels (e.g. Lee *et al.* 2000*a*,*b*). A more complex case involves Ca^{2+} liberation from intracellular stores through IP_3Rs. The opening of these channels shows dual positive and negative regulation by cytosolic Ca^{2+} (Iino, 1990; Finch *et al.* 1991; Bezprozvanny *et al.* 1991; Mak *et al.* 1998), leading to a mechanism of CICR whereby small elevations of cytosolic $[Ca^{2+}]$ promote channel opening to liberate further Ca^{2+}. Buffers are thus expected to exert a powerful effect on signals arising through intracellular Ca^{2+} liberation, as they will affect not only the fate of Ca^{2+} ions already deposited into the cytosol, but also influence the subsequent liberation of Ca^{2+} by modulating feedback onto IP_3Rs.

IP_3-evoked Ca^{2+} signals display complex spatial and temporal patterning. Stimulation by relatively high $[IP_3]$ typically gives rise to repetitive, propagating Ca^{2+} waves (Lechleiter & Clapham, 1992). Lower $[IP_3]$ evokes transient, localized Ca^{2+} elevations, christened 'Ca^{2+} puffs', which have been visualized in oocytes and other cell types (Yao *et al.* 1995; Bootman *et al.* 1997). Puffs are believed to arise because localized CICR causes the concerted opening of channels within localized clusters of a few tens of IP_3Rs, which act as functionally discrete Ca^{2+} release units (Callamaras *et al.* 1998*a*,*b*; Swillens *et al.* 1999). Puffs may serve both as local Ca^{2+} signals in their own right, and as 'building blocks' from which Ca^{2+} waves are generated. When $[IP_3]$ is sufficiently high, Ca^{2+} diffusing from one release site triggers CICR at neighbouring sites a few

Table 1. Summary of kinetic parameters and diffusion distances for binding and unbinding of Ca^{2+} to EGTA and BAPTA

	EGTA	BAPTA
Apparent K_d (nM) (at pH 7.2)	150	160
K_{on} (μM^{-1} s^{-1})	3–10	100–1000
K_{off} (s^{-1})	0.5–1.5	16–160
τ_{dwell} (ms)	700–2000	6–60
$d_{shuttle}$ (μm)	28–50	3–9
$\tau_{capture}$ (ms) (for B = 270 μM)	4–10	0.04–0.4
$d_{capture}$ (μm) (for B = 270 μM)	0.7–1	0.07–0.2

Apparent affinities (Morris *et al.* 1999) and lower and upper estimates for on-rates (K_{on}) (Naraghi, 1997; Nagerl *et al.* 2000), were used to derive off-rates ($K_{off} = K_d K_{on}$) for EGTA and BAPTA. Dwell time (τ_{dwell}) reflects how long Ca^{2+} will remain bound to each buffer, where $\tau_{dwell} = 1/K_{off}$. The corresponding mean distances over which the Ca^{2+}–buffer complex will diffuse before releasing bound Ca^{2+} ($d_{shuttle}$) were estimated as $\sqrt{(6D_{Cabuffer}\tau_{dwell})}$, assuming a diffusion coefficient ($D_{Cabuffer}$) of 200 μm^2 s^{-1}. Mean capture times before a Ca^{2+} ion binds to EGTA or BAPTA were calculated as $\tau_{capture} = 1/(K_{on}B)$ (Stern, 1992; Roberts, 1994), where B is the concentration of Ca^{2+}-free binding sites on the buffer, assuming that Ca^{2+} ions in the cytosol are bound to immobile endogenous buffers for 90 % of the time. The corresponding mean distances that a Ca^{2+} ion would diffuse before capture ($d_{capture}$) were calculated as $d_{capture} = \sqrt{(D_{Ca}\tau_{capture})}$, assuming an apparent diffusion coefficient (D_{Ca}) of 20 μm^2 s^{-1} for Ca^{2+} in the presence of immobile endogenous buffers.

microns away, giving rise to saltatory waves propagating from site to site (Yao *et al.* 1995; Bootman *et al.* 1997; Berridge, 1997; Callamaras *et al.* 1998*a*,*b*). Thus, Ca^{2+} diffusion and feedback onto the IP_3R act over two very different distance scales: rapid (microsecond) interactions over nanometre scales between individual IP_3Rs within a cluster to generate local Ca^{2+} puffs, and slower (tens of milliseconds) interactions over micrometre scales between release sites to generate global Ca^{2+} waves.

In this paper, we studied how Ca^{2+} buffers with differing kinetics modulate Ca^{2+} interactions over these widely divergent distance and time scales. Our objectives were to: (1) explore how cells might employ buffers to shape Ca^{2+} signals for their specific purposes, and (2) use buffers as a tool to derive mechanistic information about Ca^{2+} interactions at scales otherwise inaccessible to direct visualization.

We utilized *Xenopus* oocytes as a model cell system to image the perturbations of Ca^{2+} signalling resulting from intracellular injections of two mobile buffers, EGTA and BAPTA. The oocyte has advantages that intracellular Ca^{2+} liberation is mediated solely through type 1 IP_3Rs (Parys *et al.* 1992); its large size greatly facilitates intracellular injections; and it is among the best characterized cells for Ca^{2+} signalling. EGTA and BAPTA were selected for study because these well-characterized exogenous buffers display similar affinities yet have very different Ca^{2+} binding kinetics (Tsien, 1980). EGTA has an on-rate (~3–10 μM^{-1} s^{-1}: Table 1) sufficiently fast to bind Ca^{2+} ions diffusing over the micrometre distances between Ca^{2+} release sites (Roberts *et al.* 1994; Horne & Meyer, 1997; Song *et al.* 1998; Kidd *et al.* 1999), but too slow to influence short range feedback of Ca^{2+} between individual IP_3Rs at individual puff sites. On the other hand, BAPTA has a much faster on-rate (100–1000 μM^{-1} s^{-1}: Table 1) and, whereas it is expected to disrupt local Ca^{2+} feedback within IP_3R clusters, it may actually enhance coupling between release sites by acting as a 'shuttle buffer' (Stern, 1992; Roberts, 1994). We show here that injection of the slow buffer EGTA into the oocyte promotes a 'balkanization' of Ca^{2+} liberation as transient, autonomous local release events, whereas the fast buffer BAPTA results in a 'globalization' of spatially diffuse Ca^{2+} signals. Moreover, these spatial changes are accompanied by profound changes in kinetics of Ca^{2+} signals, suggesting that Ca^{2+} interactions between release sites play a large part in setting the duration of Ca^{2+} spikes.

METHODS

Preparation of *Xenopus* oocytes

Xenopus laevis were anaesthetized by immersion in 0.17 % MS-222 for 15 min and killed by decapitation in adherence with protocols approved by the UC Irvine Institutional Animal Care and Use Committee. Oocytes (stage V–VI) were manually plucked and collagenase-treated (0.5 mg ml^{-1} for 30 min) before storage in Barth's solution (composition (mM): NaCl, 88; KCl, 1; $NaHCO_3$, 2.4; $MgSO_4$, 0.82; $Ca(NO_3)_2$, 0.33; $CaCl_2$, 0.41; Hepes, 5; pH 7.4) containing 0.1 mg ml^{-1} gentamicin at 17 °C for 1–7 days before use.

Microinjection of oocytes

Intracellular microinjections were performed using a Drummond microinjector. Oocytes were first loaded with Oregon Green 488 BAPTA 1 (OG-1) together with caged IP_3 (D-*myo*-inositol 1,4,5-trisphosphate, $P_{4(5)}$-(1-(2-nitrophenyl)ethyl) ester) to respective final intracellular concentrations of 48 and 8 μM; assuming 1 μl cytosolic volume. After allowing 30 min for intracellular distribution, control Ca^{2+} responses were imaged. A specified volume of buffer solution was then injected through a fresh micropipette and the pipette was immediately removed to minimize leakage. Ca^{2+} responses were then imaged after allowing ~20 min for intracellular equilibration of buffer concentration, and sequential injections and recordings were made in this way to examine the effects of stepwise increases in buffer concentration. Injection solutions contained 5 mM of either EGTA or BAPTA together with 2.5 mM $CaCl_2$ (pH 7.25, with KOH), such that the buffers were half-saturated with Ca^{2+}. To obtain high final intracellular concentrations (> 270 μM), stock buffer concentrations were increased to 10 mM (including 5 mM $CaCl_2$) and buffer was administered by a series of repeated 10 nl injections. Control experiments, where high cytosolic buffer concentrations were attained following single injections of EGTA or BAPTA, gave similar results to those where the concentration was raised in a stepwise manner. Moreover, responses evoked in control oocytes (not injected with buffer) remained consistent over periods up to 3 h.

Confocal laser scanning microscopy

Confocal Ca^{2+} images were obtained using a custom-built line-scan confocal scanner interfaced to an Olympus IX70 inverted microscope (Parker *et al.* 1997). Recordings were made at room temperature, imaging in the animal hemisphere of oocytes bathed in normal Ringer solution (composition (mM): $NaCl_2$, 120; KCl, 2; $CaCl_2$, 1.8; Hepes, 5; pH 7.3). The laser spot of a 488 nm argon ion laser was focused with a ×40 oil immersion objective (NA 1.35) and scanned every 16 ms along a 50 μm line, of which representative trimmed sections are shown in the figures. Emitted fluorescence was detected at wavelengths > 510 nm through a confocal pinhole providing lateral and axial resolutions of about 0.3 and 0.5 μm, respectively. The scan line was focused at the level of the pigment granules and images were collected through a coverglass forming the base of the recording chamber. Fluorescence signals are expressed as ratios (F/F_0 or $\Delta F/F_0$) of the fluorescence (F) at each pixel relative to the mean resting fluorescence (F_0) at that pixel prior to stimulation. IP_3 was photo-released from a caged precursor by delivering flashes of UV light, focused uniformly throughout a 200 μm spot surrounding the image scan line (Callamaras & Parker, 1998). The amount of photo-released IP_3 was controlled (in a linear manner) by varying flash duration. Each flash consumes only a negligible fraction of the caged IP_3 (Callamaras & Parker, 1998), thus it was possible to acquire numerous consistent responses using repeated flashes. Intervals of > 60 s were allowed between recordings to allow IP_3Rs to recover from desensitization and for cytosolic $[Ca^{2+}]$ to recover to basal levels. Images were constructed and processed using custom routines written in the IDL programming environment (Research Systems, Boulder, CO, USA), and measurements were exported to Microcal Origin 6.0 (OriginLab, Northampton, MA, USA) for analysis and graphing.

Expression of N-type Ca^{2+} channels

Plasmids containing cDNA clones coding for the N-type Ca^{2+} channel α_{1B-d} and β_3 subunits (Lin *et al.* 1997) were linearized and transcribed *in vitro*. Equal quantities of each subunit cRNA were mixed to a final concentration of 0.1–1 $\mu g\ \mu l^{-1}$ and injected (50 nl) into defolliculated oocytes 3–5 days prior to imaging and electrophysiological recording. Membrane potential was held at −60 mV using a two-electrode voltage clamp (Gene Clamp 500, Axon Instruments, Foster City, CA, USA), and stepped to +30 mV

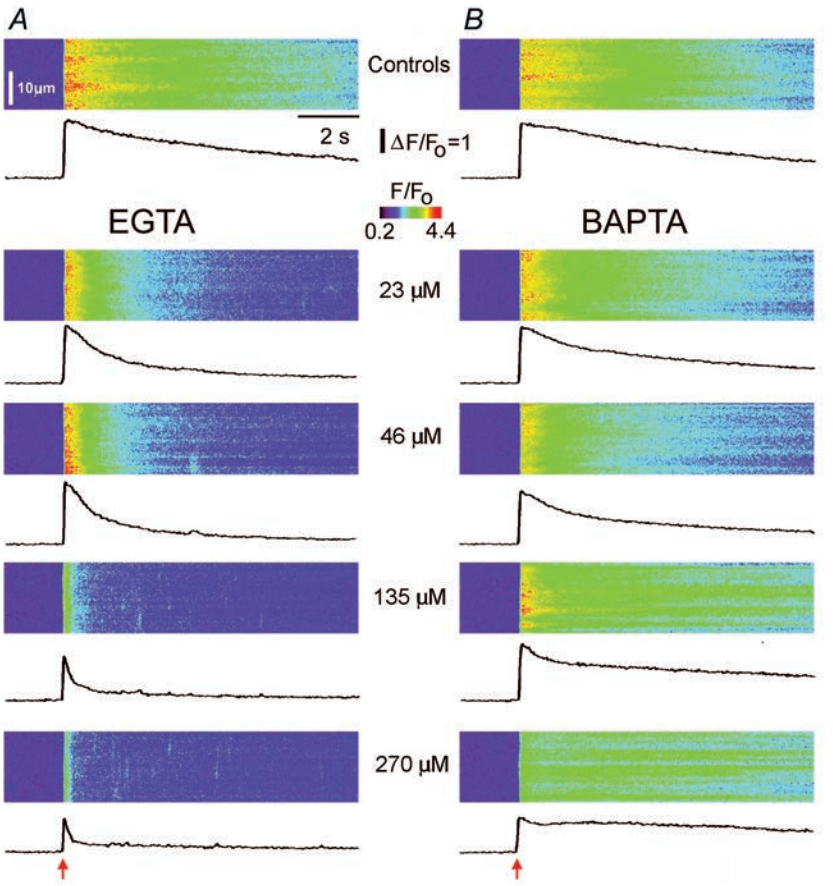

Figure 1. Modulation of IP_3-evoked Ca^{2+} signals by EGTA and BAPTA

Confocal line-scan images illustrate Ca^{2+} signals evoked by photoreleased IP_3 in the presence of increasing concentrations of buffer. In each image, distance is depicted vertically, time runs from left to right and increasing Oregon Green 488 BAPTA 1 (OG-1) fluorescence ratio ($\Delta F/F_0$: proportional to $[Ca^{2+}]_{free}$) is represented by 'warmer' colours as denoted by the colour bar. Identical photolysis flashes (normalized intensities of 1.5 in *A* and 1.9 in *B*) were delivered at the arrows. Traces below each image show fluorescence profiles averaged over 100 pixel (6.6 μm) regions. *A*, upper panel shows response before loading buffer, and subsequent panels illustrate responses after sequentially loading the same oocyte with EGTA to the final intracellular concentrations stated. *B*, similar records from a different oocyte showing the effects of increasing concentrations of BAPTA.

to induce opening of N-type Ca^{2+} channels expressed in the plasma membrane. Ca^{2+} imaging was as described above, except that $[Ca^{2+}]$ in the Ringer solution was 6 mM.

Reagents

OG-1, caged IP_3 and BAPTA were from Molecular Probes Inc. (Eugene, OR, USA); all other reagents were from Sigma Chemical Co. (St Louis, MO, USA).

RESULTS

Actions of buffers on IP_3-evoked Ca^{2+} signals

We compared the actions of fast (BAPTA) and slow (EGTA) Ca^{2+} buffers on IP_3-evoked intracellular Ca^{2+} signals. *Xenopus* oocytes were loaded with the indicator OG-1 together with caged IP_3, and confocal line-scan images of Ca^{2+}-dependent fluorescence were acquired along a 50 μm scan line focused ~5 μm inward from the cell surface where Ca^{2+} release sites are concentrated (Callamaras & Parker, 1999). IP_3 was photo-released by UV light flashes, with durations set by an electronic shutter to provide a linear control of the relative amount of IP_3 liberation. To control for variation between oocytes, flash strengths were normalized relative to that evoking a half-maximal response under control conditions (i.e. before adding buffer) in each cell.

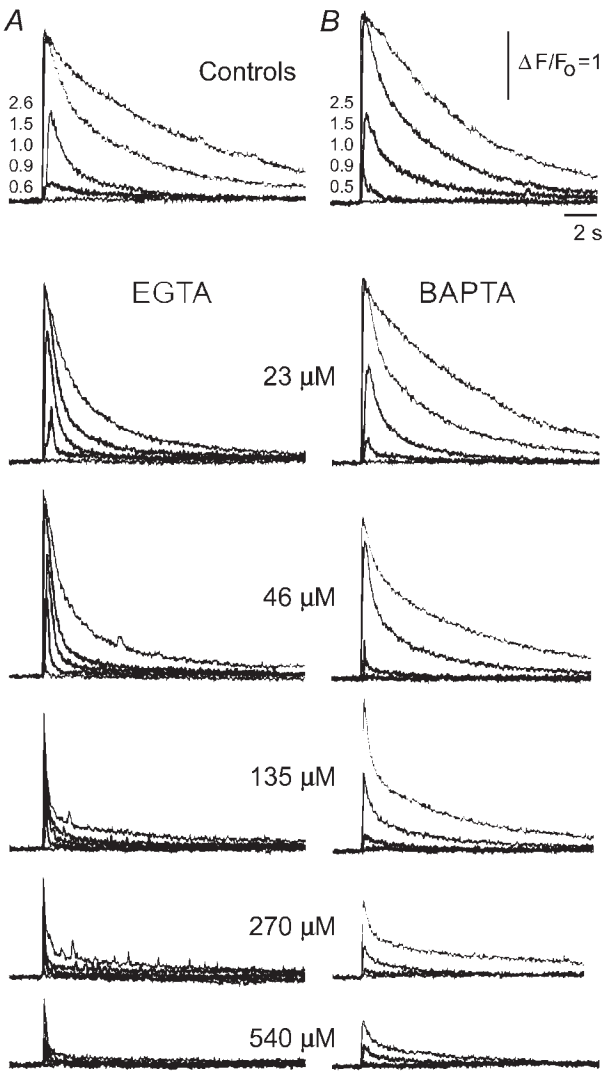

Figure 2. Buffer actions at varying $[IP_3]$

Representative fluorescence profiles (from different oocytes to those in Fig. 1) show superimposed Ca^{2+} transients evoked by increasing photorelease of IP_3 in the absence of exogenous buffer (upper panels) and after loading increasing concentrations of EGTA (*A*) or BAPTA (*B*). Traces correspond to different photolysis flash strengths, indicated in normalized units.

Figure 1 illustrates Ca^{2+} images obtained at various buffer concentrations in response to a fixed flash strength, and Fig. 2 shows superimposed fluorescence traces in response to various flash strengths at each buffer concentration. Following acquisition of control records (upper panels in Figs 1 and 2), a volume of buffer solution (EGTA, Figs 1*A* and 2*A*; or BAPTA, Figs 1*B* and 2*B*) was injected into each oocyte to give a final intracellular concentration of 23 μM (see Methods for details). Microinjection pipettes were removed immediately following injection to prevent leakage, and oocytes were left for ~20 min to ensure uniform buffer distribution and re-equilibration of Ca^{2+} ions in the cytosol before imaging responses to the same series of UV flashes. This procedure was then repeated, sequentially injecting increasing volumes of buffer solutions to image Ca^{2+} signals at progressively higher buffer concentrations (46–540 μM).

The data in Figs. 1 and 2 are representative of observations in 45 oocytes (EGTA, $n = 21$; BAPTA, $n = 24$). The results are analysed in the following sections, but the most striking finding was that EGTA (a Ca^{2+} buffer with slow Ca^{2+} binding kinetics) greatly abbreviated IP_3-evoked Ca^{2+} signals, whereas BAPTA (a faster Ca^{2+} buffer) slowed their decay.

Changes in Ca^{2+} signals result from increased buffering, not changes in resting $[Ca^{2+}]$ or store content

The effects described in Figs 1 and 2 might, in principle, arise either through buffering of Ca^{2+} liberated in response to IP_3, or because the added buffers chelated oocyte Ca^{2+} to cause long-term changes in basal cytosolic free $[Ca^{2+}]$ or in the loading of Ca^{2+} stores. Observations that equal amounts of two buffers of similar affinity produced dissimilar effects already suggested that the latter possibilities were not the case. Moreover, experiments were carried out by injecting each buffer already half-saturated with Ca^{2+}, so that the free $[Ca^{2+}]$ in the injection solutions would have been ~150 nM, a little higher than basal free $[Ca^{2+}]$ in the oocyte cytosol (Yao *et al.* 1995). As an additional control, we repeated the experiments using solutions of EGTA and BAPTA that contained either no added Ca^{2+} or were saturated (1:1 ratio) with Ca^{2+}. The results were essentially identical to those in Figs 1 and 2 (data not shown), indicating that the effects of EGTA and BAPTA on Ca^{2+} signals did not result from addition or removal of available Ca^{2+} ions within the oocyte.

Positive and negative modulation of IP_3-evoked Ca^{2+} signals by buffers

Figure 3*A* and *B* shows families of curves plotting the mean peak amplitude of fluorescence signals evoked by increasing photorelease of IP_3 at various concentrations of EGTA and BAPTA, respectively. High cytosolic concentrations (> 135 μM) of both buffers appreciably reduced the amplitude of Ca^{2+} signals evoked by strong photorelease of IP_3, with BAPTA being more potent than EGTA. This reduction was expected – in part because the buffers will compete with indicator dye for free Ca^{2+} ions. In contrast, Ca^{2+} signals evoked by weak photolysis flashes were potentiated by EGTA; as shown in Fig. 3*C*, plotting Ca^{2+} signals evoked by weak (0.6–0.8) and strong (1.9–2.6) flashes at various buffer concentrations relative to control responses without added buffer. Potentiation was strongest at low (< 300 μM) concentrations of EGTA, but responses remained greater than control values at concentrations as high as 2 mM EGTA. The slow binding kinetics of EGTA appear to be important for this effect, because little potentiation was apparent with corresponding concentrations of BAPTA (Fig. 3*D*).

Buffers reduce the apparent cooperativity of IP_3-evoked Ca^{2+} liberation

The concentration–response relationships in Figs 3*A* and *B* are fitted by Hill curves ($y = V_{max}(x^{n_H}/(k^{n_H} + x^{n_H})$: where y = peak fluorescence ratio ($\Delta F/F_0$) at any given [IP_3] (x); V_{max} = peak $\Delta F/F_0$ at saturating [IP_3]; and n_H is the Hill coefficient, which gives a measure of the apparent cooperativity of IP_3 action in evoking Ca^{2+} liberation. Data from these curves are plotted in Fig. 4, showing the dependence of n_H (Fig. 4*A*) and V_{max} (Fig. 4*B*) on concentration of EGTA or BAPTA.

The steep dependence of Ca^{2+} liberation on [IP_3] is likely to arise both from the requirement for binding to more than one subunit of the tetrameric receptor for channel opening and because of positive cooperativity resulting from CICR (Meyer *et al.* 1990; Hirota *et al.* 1995; Marchant & Taylor, 1997; Callamaras *et al.* 1998*a*). In agreement with this dual

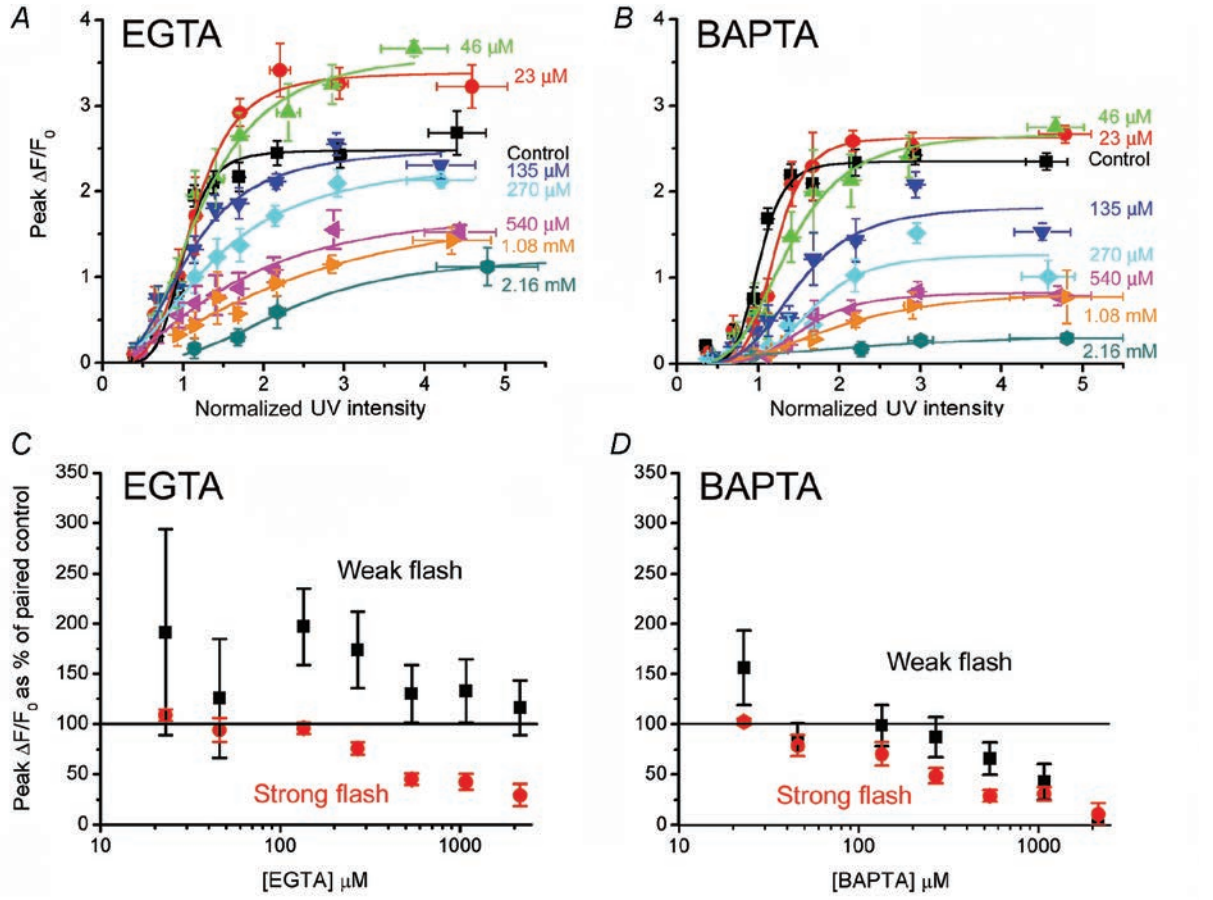

Figure 3. Buffers both facilitate and depress IP_3-evoked Ca^{2+} signals

A and *B*, mean peak amplitude ($\Delta F/F_0$) of Ca^{2+} signals as a function of photolysis flash strength, plotted for various intracellular concentrations of EGTA (*A*: n = 21 oocytes) and BAPTA (*B*: n = 24). Curves were fitted using the Hill equation. *C* and *D*, changes in peak fluorescence signal as a function of increasing [buffer] plotted as a percentage of that in the same oocyte before loading buffer. Data are pooled for weak (black symbols) and strong (red) photolysis flashes (respective normalized flash strengths 0.6–0.8 and 1.9–2.6) in the presence of EGTA (*C*, n = 14) and BAPTA (*D*, n = 17).

mechanism, n_H in control conditions (before adding buffer) was ~6.3, a value greater than expected even if channel opening requires binding to all four subunits. Moreover, progressive increases in buffer concentrations reduced n_H to a minimal value of about 2 (Fig. 4*A*). A probable interpretation is that Ca^{2+} buffers disrupt the diffusion of Ca^{2+} ions between IP_3Rs that normally leads to CICR, and that this communication contributes appreciably to the apparent cooperativity of IP_3 action. Indeed, the minimal n_H at high buffer concentrations suggests that binding of IP_3 to two (or possibly even one) subunits may be sufficient for channel opening. Finally, moderate concentrations of EGTA caused a greater reduction in n_H than equivalent concentrations of BAPTA (Fig. 4*A*). Because EGTA impairs Ca^{2+} diffusion between clusters of IP_3Rs rather than between individual IP_3Rs within a cluster (see Discussion), it seems that cluster–cluster interactions predominate in establishing the normally high cooperativity of IP_3 action.

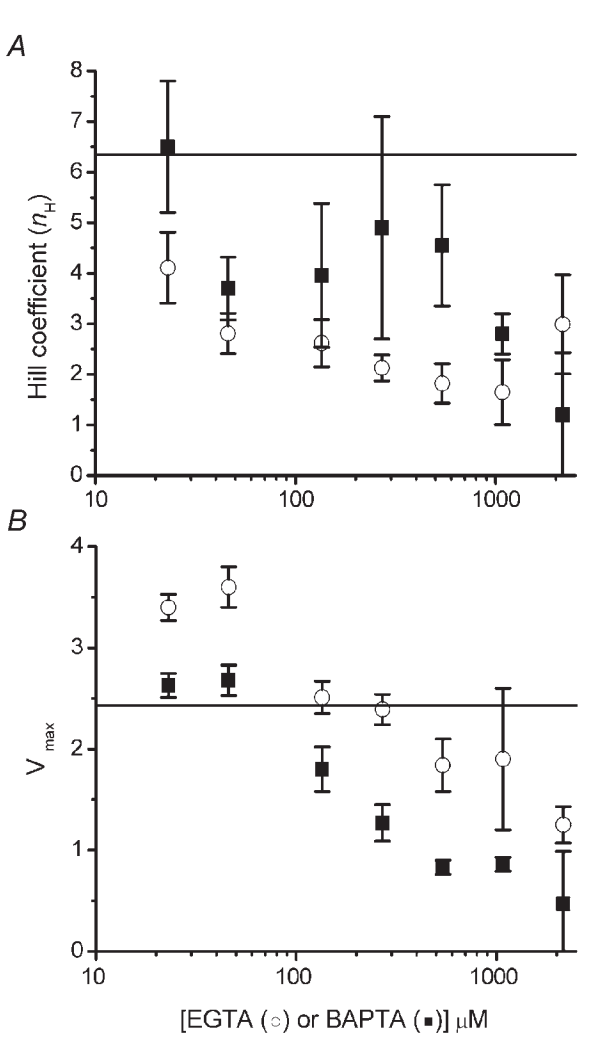

Figure 4. Ca^{2+} buffers reduce the apparent cooperativity of IP_3 action

A, Hill coefficients, derived from the curves fitted to data in Fig. 3*A* and *B*, are plotted as functions of [EGTA] (open circles) and [BAPTA] (filled squares). *B*, plot shows V_{max} (maximal fluorescence signal at infinite [IP_3] derived from Hill-fits) as functions of [EGTA] (open circles) and [BAPTA] (filled squares). Horizontal lines on each graph represent control values (i.e. no exogenous buffer).

V_{max} values derived from Hill fits provide a measure of maximal fluorescence at saturating [IP_3], and are plotted as a function of [buffer] in Fig. 4*B*. V_{max} declined progressively with increasing concentrations of BAPTA, whereas a biphasic relationship was apparent with EGTA, with an initial potentiation apparent at 23 and 46 μM EGTA.

Differential effects of buffers on kinetics of IP_3-evoked Ca^{2+} signals

As noted earlier, EGTA and BAPTA exerted very different actions on the kinetics of IP_3-evoked Ca^{2+} transients; respectively causing an acceleration or prolongation of their decay. This is illustrated in Fig. 5*A*, showing superimposed responses to strong photolysis flashes in the presence of increasing [EGTA] or [BAPTA] after normalizing amplitudes to facilitate comparison. Fluorescence decays were fit by mono- or bi-exponential curves (Fig. 5*B*). In the absence of exogenous buffer, the decay followed a single exponential, with a time constant (τ_{slow}) of a few seconds that slowed progressively with increasing photorelease of IP_3. In the presence of EGTA the decay phase became markedly biphasic (Fig. 5*B*), with a prominent fast component (τ_{fast}) and smaller slower component (τ_{slow}). In the presence of BAPTA a slow decay was prominent, and some oocytes (13/20) also showed a small fast component (Fig. 5*B*).

Figure 6 shows measurements of time constants of the fast and slow decay components, and their relative weights in contributing toward the overall decline in [Ca^{2+}], plotted as a function of flash strength for various concentrations of EGTA or BAPTA. Several features are evident. (1) In the absence of added buffer, Ca^{2+} transients showed a mono-exponential decay with a time constant slowing from ~1 s with just-suprathreshold photorelease of IP_3 to nearly 10 s with stronger photo-release (black symbols, Fig. 6*A*–*D*). (2) EGTA caused the decay to become markedly biphasic, with an initial fast decline (τ_{fast}) that contributed > 80 % of the total decay (Fig. 6*E*) and shortened with increasing [EGTA] (Fig. 6*A*). The value of τ_{fast} slowed with increasing [IP_3] at low (< 50 μM) concentrations of EGTA, but was relatively independent of [IP_3] at high (> 135 μM) concentrations of EGTA (Fig. 6*A*). Following the large, fast decay, the remaining small component declined with a time constant (τ_{slow}) that lengthened slightly with increasing photorelease of IP_3, and was slower than in the absence of added buffer (Fig. 6*C*). (3) Addition of BAPTA greatly slowed (τ_{slow} 10–30 s) the major part of the Ca^{2+} signal (Fig. 6*D*). In those oocytes that displayed biphasic kinetics, the initial fast component was much smaller than with EGTA (Fig. 6*E*), and its time constant (τ_{fast}) was faster than in controls, but slower than with EGTA (Fig. 6*B*).

Decay of Ca^{2+} transients is dominated by release kinetics, not sequestration

IP_3-evoked Ca^{2+} signals reflect a balance between Ca^{2+} liberation through IP_3Rs into the cytosol and its subsequent removal by processes including buffering, extrusion, re-sequestration via sarco(endo)plasmic reticulum Ca^{2+}-ATPase (SERCA) pumps and diffusion into the enormous interior volume of the oocyte (Parker *et al.* 1996). The differing effects of EGTA and BAPTA on the kinetics of Ca^{2+} signals (Fig. 6) might thus arise either through modulation of Ca^{2+} liberation or through actions on subsequent cytosolic Ca^{2+} clearance. To discriminate between these possibilities, we examined the effects of buffers on signals arising from Ca^{2+} flux into the cytosol through voltage-gated N-type Ca^{2+} channels expressed in the plasma membrane. Opening of these channels by a depolarizing pulse is expected to induce a fixed 'pulse' of Ca^{2+} influx – without complications of CICR as with IP_3Rs – and the decay of the resulting Ca^{2+} transient should thus provide a good measure of cytosolic Ca^{2+} clearance. Moreover, the spatial distribution of Ca^{2+} influx across the plasma membrane is expected to closely mimic Ca^{2+} liberation from IP_3-sensitive sites, as these are distributed as a thin shell close under the membrane (Callamaras & Parker, 1999). Ca^{2+} arising from both sources will thus approximate a 2-dimensional sheet, with subsequent diffusion along a radial axis into the interior of the oocyte.

Oocytes expressing N-type channels were voltage clamped at −60 mV and stepped to +30 mV for 300 ms to induce Ca^{2+} influx with a duration matching the rise time of IP_3-evoked Ca^{2+} signals (Fig. 7). After the fluorescence signal had returned to baseline (10 s), a UV flash was applied to photorelease IP_3 (red arrow). Before loading Ca^{2+} buffers, signals induced by activation of N-type Ca^{2+} channels decayed much more rapidly than those evoked by IP_3, even though they were of similar amplitude (Fig. 7*A*). This marked disparity indicates that the slow decay of the IP_3-evoked signals did not arise through dye saturation – a conclusion further supported by findings of similar decay rates with the low affinity (K_d ~4 μM) indicator Fluo-4 dextran (not shown).

Thus, the decay of IP_3-evoked signals does not simply reflect Ca^{2+} clearance, but instead is determined primarily by a persistent liberation of Ca^{2+} through IP_3Rs lasting for several seconds. Furthermore, the effects of EGTA and BAPTA are most readily explained by their actions on this prolonged Ca^{2+} liberation, rather than on Ca^{2+} clearance from the cytosol. Both EGTA (Fig. 7*B*) and BAPTA (Fig. 7*C*) produced only a modest speeding of decay of signals resulting from Ca^{2+} influx through N-type channels, in marked contrast to their respective actions to accelerate or slow IP_3-evoked Ca^{2+} signals.

Biphasic Ca^{2+} liberation through IP_3Rs

Data from experiments similar to those in Fig. 7 were then used to derive the kinetics of Ca^{2+} flux into the cytosol through IP_3R, assuming that subsequent Ca^{2+} clearance follows a first order process with a rate constant (k) corresponding to the decay of Ca^{2+} signals following influx

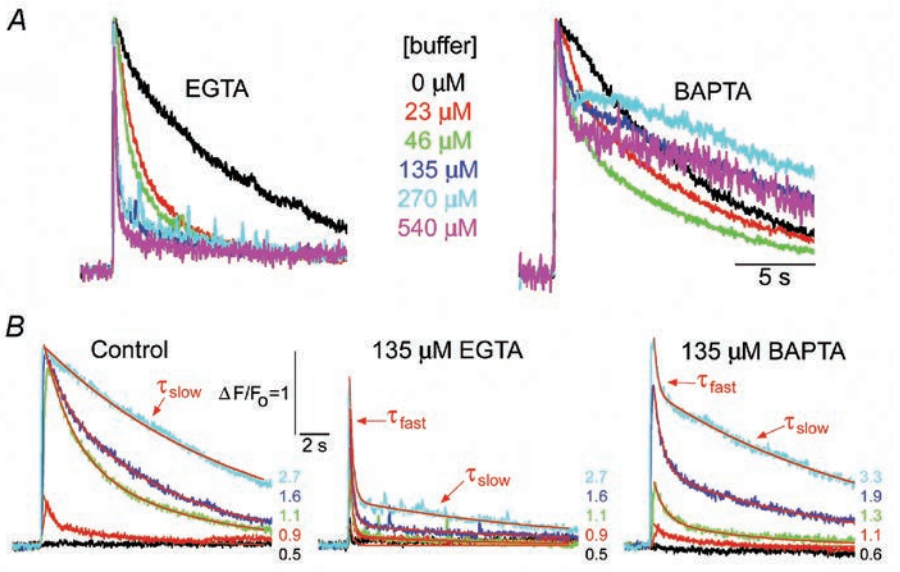

Figure 5. Ca^{2+} transients are speeded by EGTA but prolonged by BAPTA

A, families of curves illustrate Ca^{2+} transients evoked by a fixed photolysis flash (normalized strength 2.5) in the presence of the indicated concentrations of EGTA (left) and BAPTA (right). Responses are scaled to same peak height to facilitate comparison. *B*, Ca^{2+} transients evoked by various photolysis flashes of various strengths (normalized strengths indicated) before loading buffer (left); in the same oocyte after loading 135 μM EGTA (middle); and in a different oocyte loaded with 135 μM BAPTA (right). Red curves illustrate fitting of single or double exponentials to derive fast (τ_{fast}) and slow (τ_{slow}) decay time constants.

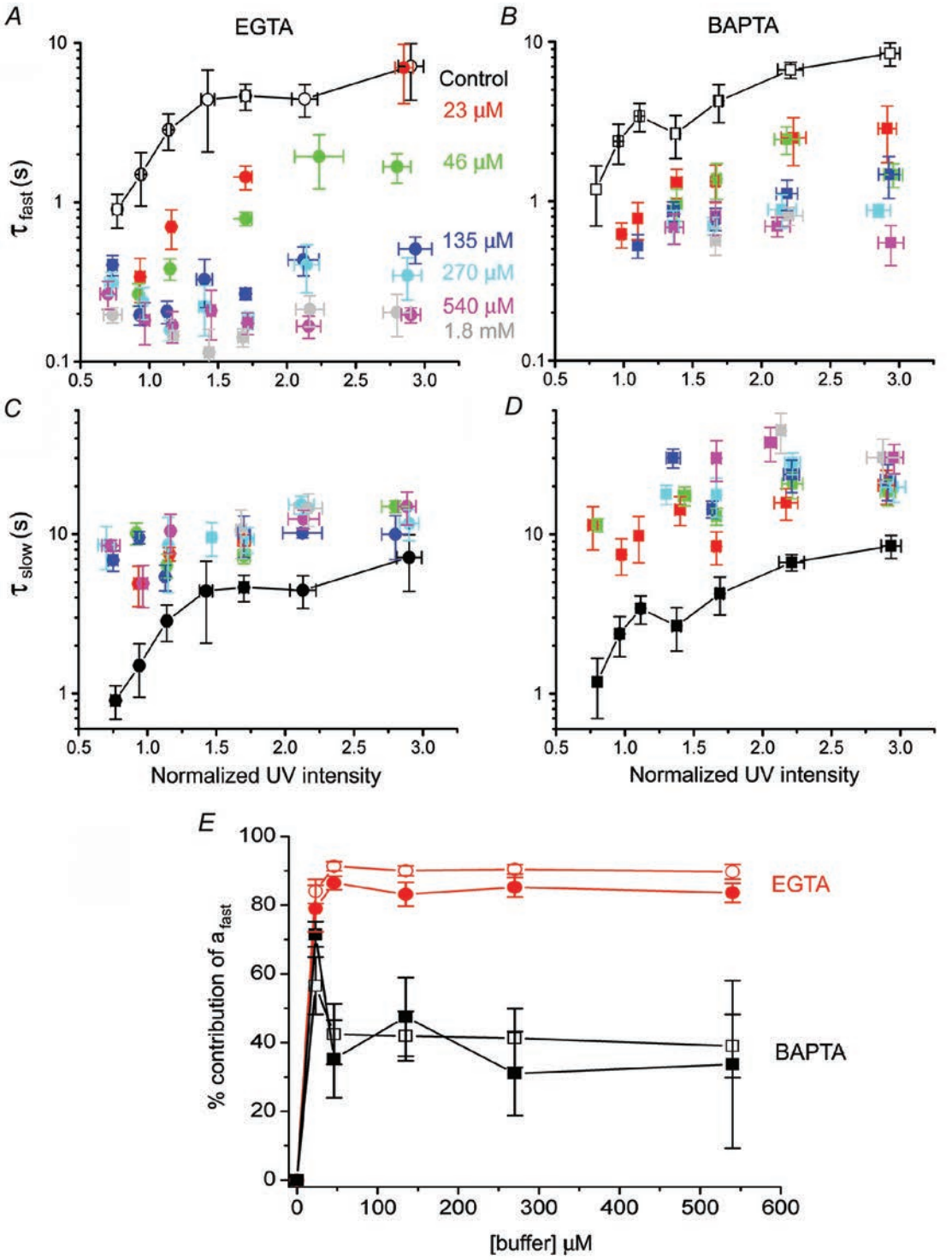

Figure 6. EGTA and BAPTA differentially affect the fast and slow decay components of IP_3-evoked Ca^{2+} transients

A and *C*, graphs show, respectively, the time constants for the fast (τ_{fast}) and slow (τ_{slow}) decay components as a function of photolysis flash strength, in the presence of various concentrations of EGTA. *B* and *D*, similar data, with corresponding concentrations of BAPTA. Because the decay of Ca^{2+} transients without added buffer was mono-exponential, control time constants are repeated in the upper and lower panels (black symbols joined by lines). *E*, plot shows the relative magnitude of the fast decay component (τ_{fast}: measured as shown in Fig. 5*B*) at various concentrations of EGTA (red symbols) and BAPTA (black symbols). The amplitudes of the fast and slow components (a_{fast} and a_{slow}, respectively) were derived at the time of the peak signal from bi-exponential fits, and the graph shows the percentage contribution of a_{fast} to the total signal (i.e. $a_{fast}/(a_{fast} + a_{slow}) \times 100$). Open and filled symbols represent signals evoked, respectively, by weak and strong photolysis flashes.

through N-type channels (Fig. 8). Ca^{2+} flux from intracellular stores is thus proportional to $d[Ca^{2+}]/dt + k[Ca^{2+}]$, where $[Ca^{2+}]$ is the free cytosolic Ca^{2+} concentration as signalled by changes in fluorescence (Parker *et al.* 1996). Consistent with previous observations (Parker *et al.* 1996), control oocytes showed an initial fast spike of IP_3-evoked Ca^{2+} liberation, followed by a lingering 'tail' of Ca^{2+} efflux persisting for several seconds (upper traces, Fig. 8*B* and *D*). Although the tail component is small (Fig. 8*A* and *C*), over time it contributes one-half or more of the total Ca^{2+} liberated, and is responsible for the prolonged Ca^{2+} transients evoked by IP_3 under normal conditions. EGTA almost abolished the tail component of Ca^{2+} liberation (Fig. 8*B*), thus accelerating the decay of the fluorescent Ca^{2+} profile (Fig. 8*A*). Different to this, the tail component was not significantly altered by BAPTA (Fig. 8*D*), suggesting that prolonged release of Ca^{2+} through the IP_3R may involve cluster–cluster interactions that are selectively disrupted by slow buffers.

Changes in spatial distribution of Ca^{2+} signals

In addition to their actions on the amplitude and kinetics of IP_3-evoked Ca^{2+} signals, EGTA and BAPTA produced characteristic, and very different, changes in the spatial distribution of Ca^{2+} signals (Fig. 9). Control oocytes (without added buffer) often display transient localized Ca^{2+} signals (puffs) in response to photolysis flashes within a narrow 'window' of flash strengths (Yao *et al.* 1995), but these were not evident in the oocytes illustrated, and only spatially diffuse Ca^{2+} waves were observed (Fig. 9*A*). However, following injection of EGTA (135 μM), the same oocytes showed discretely localized puffs (Fig. 9*B*: representative of 14/15 oocytes). With weak stimuli puffs arose at discrete sites following differing latencies. Stronger photorelease of IP_3 caused sites to respond almost simultaneously, giving rise to the abrupt, rapidly decaying Ca^{2+} transient described earlier. Puffs continued after this initial transient and became more frequent, but smaller, with progressively stronger stimuli. In marked contrast, the same concentration (135 μM) of BAPTA abolished Ca^{2+} responses to weak photolysis flashes (10/18 oocytes with normalized flash strengths $\leqslant$1.1), and at higher flash strengths oocytes showed only spatially uniform and slowly decaying Ca^{2+} signals. We never (0/24 oocytes) observed localized Ca^{2+} puffs.

DISCUSSION

We show that two mobile Ca^{2+} buffers with similar affinities but very different binding kinetics affect the spatiotemporal characteristics of IP_3-evoked Ca^{2+} liberation in contrasting ways. EGTA – a buffer with a slow binding rate – causes Ca^{2+} signals to become more transient and 'balkanizes' Ca^{2+} liberation such that individual release sites act autonomously to generate discrete puffs rather than functioning in concert to generate Ca^{2+} waves. On the other hand, BAPTA – a fast buffer – prolongs Ca^{2+} transients and promotes a 'globalization' of Ca^{2+} signalling as a spatially

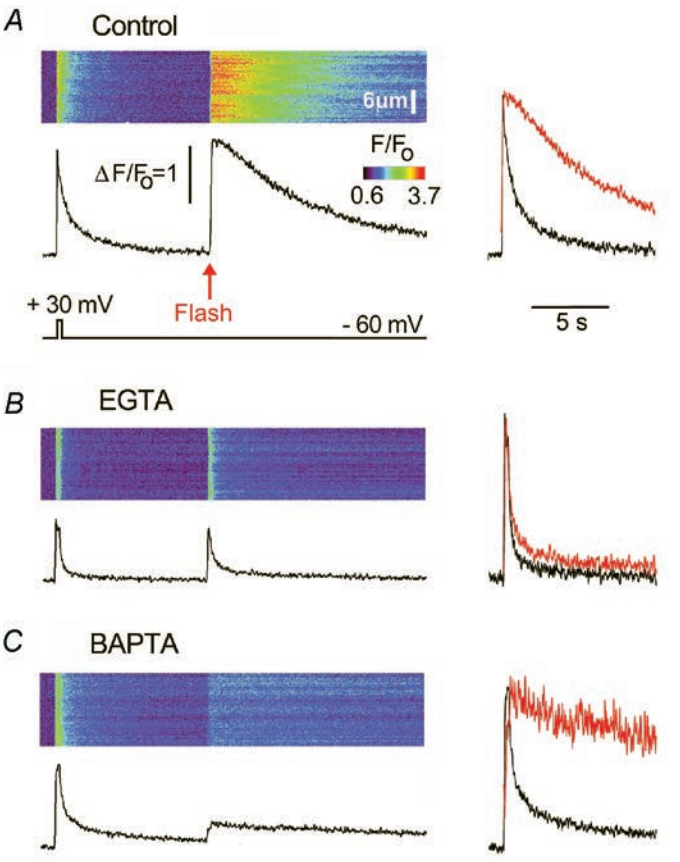

Figure 7. The decay of IP_3-evoked Ca^{2+} transients is largely determined by the kinetics of Ca^{2+} release, not sequestration

A, line-scan image shows a Ca^{2+} transient evoked by a 300 ms duration depolarization to +30 mV to activate expressed N-type channels, followed 10 s later by a UV flash to photorelease IP_3. The lower trace shows the fluorescence profile averaged across a 6.6 μm region of the scan line, and superimposed traces on the right compare the voltage-gated signal (black) with the IP_3-evoked signal (red) after normalizing to the same peak height. *B*, corresponding image and traces recorded under identical conditions in the same oocyte after loading 270 μM EGTA. *C*, similar records in a different oocyte loaded with 270 μM BAPTA. Control records in this oocyte before loading BAPTA were similar to one in *A*.

uniform elevation without evidence of local release events. These strikingly different actions cannot be explained merely by chelation of Ca^{2+} subsequent to its liberation into the cytosol, because Ca^{2+} signals generated by influx through voltage-gated channels were affected to a much lesser degree by EGTA and BAPTA (Fig. 7). Moreover, they do not arise through changes in resting free [Ca^{2+}] or alterations in Ca^{2+} store filling, as similar results were obtained whether buffers were injected either without Ca^{2+} or saturated with Ca^{2+}. Instead, EGTA and BAPTA appear to act over different time and distance scales to modulate the processes of Ca^{2+} diffusion and CICR that shape the regenerative nature of IP_3-evoked Ca^{2+} liberation.

Spatiotemporal scales of Ca^{2+} signalling

IP_3Rs are organized in *Xenopus* oocytes as tight (*ca* 50 nm diameter) clusters containing several tens of channels, with a mean cluster–cluster spacing of ~3 μm (Callamaras *et al.* 1998*a*,*b*; Swillens *et al.* 1999; Shuai & Jung, 2002, 2003). CICR can thus act over two very different spatiotemporal scales – via fast diffusion over nanometre distances between IP_3Rs within a cluster to give local Ca^{2+} puffs, and much more slowly across micrometre distances between clusters to generate propagating saltatory waves (Fig. 10*A*: Yao *et al.* 1995; Bootman *et al.* 1997; Berridge, 1997; Callamaras *et al.* 1998*a*,*b*; Marchant & Parker, 2000). Depending on their kinetics, buffers may selectively act on one or other of these processes.

Key factors determining the interactions of buffers with Ca^{2+} ions are summarized in Table 1, and include: (1) the mean time ($\tau_{capture}$) and distance ($d_{capture}$) that a Ca^{2+} ion will diffuse before it becomes bound to a buffer molecule; (2) the mean time (dwell time; τ_{dwell}) a Ca^{2+} ion will remain bound to a buffer before dissociating, and the corresponding mean distance ('shuttle' distance; $d_{shuttle}$) by which the Ca^{2+}–buffer complex will diffuse before dissociation. Further, diffusion of Ca^{2+} ions in the cytosol is slowed by binding to endogenous, immobile buffers. Less than 10 % of the total Ca^{2+} ions in the cytosol are free at any given time, and the apparent diffusion coefficient for Ca^{2+} in the oocyte is thereby slowed about 10-fold as compared to free aqueous diffusion (respectively, 20 *vs.* 200 $\mu m^2\ s^{-1}$: Allbritton *et al.* 1992; Yao *et al.* 1995). Buffers, such as EGTA and BAPTA can thus act as a 'shuttle' to facilitate diffusion (Stern, 1992; Roberts, 1994) because, when bound to a mobile buffer molecule, a Ca^{2+} ion is 'protected' from binding to immobile sites and is thus carried appreciable distances at a rate only a little slower than that for free aqueous diffusion.

Buffer actions on inter- and intra-cluster signalling

We present here a qualitative model to account for the actions of EGTA and BAPTA on IP_3-evoked Ca^{2+} signalling, which is summarized in Fig. 10. This is necessarily simplified, and will require mathematical modelling for rigorous verification, but nevertheless offers useful insights.

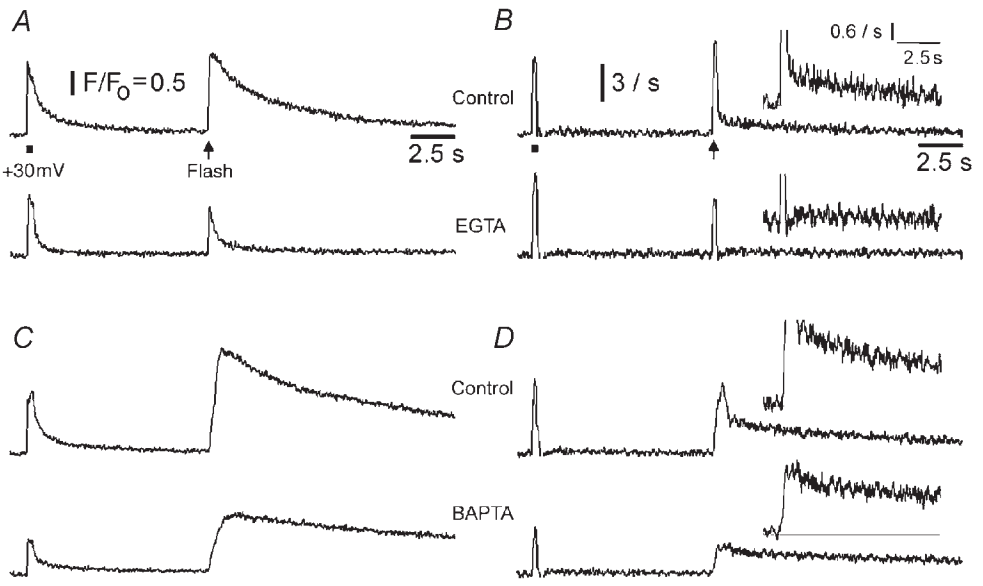

Figure 8. EGTA abolishes the 'tail' of IP_3-evoked Ca^{2+} liberation that normally prolongs Ca^{2+} transients

A, fluorescence signals evoked by Ca^{2+} entry through voltage-gated channels (bar) and by photoreleased IP_3 (arrow), before (upper) and after (lower) loading 270 μM EGTA, derived from images similar to Fig. 7*A* and *B*. *B*, rates of Ca^{2+} flux into the cytosol derived from the records in *A*, as described in the text. Traces were smoothed using 15 point adjacent averaging. Calibration bar corresponds to a rate of increase in fluorescence ($d(\Delta F/F_0)/dt$) of 3 s^{-1}. Inset graphs show the same records with expanded vertical axes to better illustrate the abolition of the persistent 'tail' of Ca^{2+} liberation by EGTA. *C* and *D*, similar data from a different oocyte, illustrating the lack of action of BAPTA (270 μM) on the tail of Ca^{2+} liberation.

Dealing first with EGTA, we consider how cytosolic diffusion of Ca^{2+} would be altered in the presence of 270 μM of this buffer. Its slow on-rate implies that a Ca^{2+} ion will diffuse an average distance of about 1 μm before binding to an EGTA molecule (Table 1). EGTA is thus expected to have little effect on short-range Ca^{2+} feedback over nanometre distances between individual IP_3Rs within a cluster, but it will efficiently capture Ca^{2+} ions diffusing over micrometre distances between neighbouring clusters (Roberts, 1994; Horne & Meyer, 1997; Song *et al.* 1998; Callamaras *et al.* 1998*a*,*b*; Kidd *et al.* 1999). Once bound, Ca^{2+} ions will be unavailable to trigger CICR for prolonged periods (τ_{dwell} = 0.7–2 s: Falcke, 2003), and Ca^{2+} bound to EGTA will be shuttled long distances ($d_{shuttle}$ = 28–50 μm) before being 'dumped' in the interior of the oocyte where release sites are absent (Callamaras & Parker, 1999). The overall effect will thus be to more sharply restrict Ca^{2+} signals around individual clusters, and reduce free [Ca^{2+}] between clusters so as to functionally uncouple them (Fig. 10*B*). In agreement, EGTA has little effect on puffs (Callamaras & Parker, 2000), yet strongly inhibits Ca^{2+} waves and dissociates global IP_3-evoked Ca^{2+} signals into discrete, localized Ca^{2+} release events (Fig. 9: Horne & Meyer, 1997; Kidd *et al.* 1999; Callamaras & Parker, 2000).

In contrast, BAPTA has an on-rate about 100 times faster than EGTA, and binds Ca^{2+} ions within a distance (tens of nanometres; Table 1) comparable to the dimensions of an IP_3R cluster, thereby reducing CICR between individual receptors within the cluster. Subsequently, Ca^{2+} bound to BAPTA will rapidly (*ca* 10 ms) be 'shuttled' a few micrometres before dissociating. This is comparable to the inter-cluster spacing, so whereas BAPTA will inhibit *intra*-cluster feedback by Ca^{2+} it may actually facilitate *inter*-cluster communication. Moreover, discrete puffs arise only when the Ca^{2+} release time at a site (*ca* 50 ms: Sun *et al.* 1998) is short in relation to the inter-cluster diffusion time (Dawson *et al.* 1999; Shuai & Jung, 2003). This condition is fulfilled in the absence of exogenous buffer, but the ability of BAPTA to rapidly shuttle Ca^{2+} and thereby speed its diffusion effectively 'smears' the distribution of Ca^{2+}, so that the endoplasmic reticulum

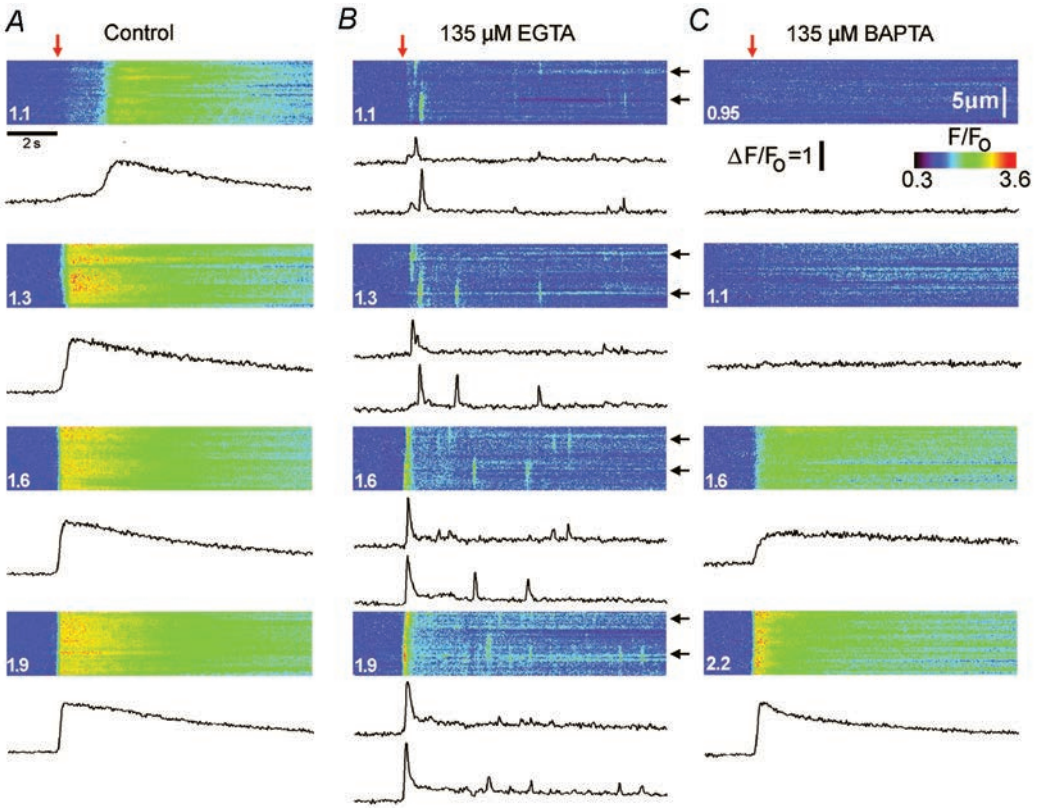

Figure 9. EGTA balkanizes Ca^{2+} signals into discrete, autonomous units, whereas BAPTA promotes spatially uniform global signals

A, line-scan images and fluorescence profiles (averaged over 4 μm regions) showing responses to photolysis flashes (red arrows) of increasing strength (indicated in normalized units) before injecting buffer. *B*, corresponding records in the same oocyte after loading 135 μM EGTA. Two representative fluorescence profiles are illustrated from each image, recorded at different puff sites (arrowed). *C*, corresponding records in a different oocyte loaded with 135 μM BAPTA. Records in this oocyte before loading BAPTA were similar to those in *A*.

(e.r.) approximates a deterministic, spatially continuous Ca^{2+} source, rather than an array of loosely coupled, discrete stochastic sources (Dawson *et al.* 1999; Shuai & Jung, 2003).

Cooperativity of IP_3-evoked Ca^{2+} release

In the absence of added buffer, Ca^{2+} liberation in the oocyte increases steeply ($n_H > 6$) with [IP_3]. This is likely to reflect both the requirement for binding of multiple IP_3 molecules to open the homo-tetrameric IP_3R, and positive cooperativity introduced by CICR. Our results suggest that the latter is the more prominent factor. High (millimolar) concentrations of both EGTA and BAPTA reduced n_H to ~2, suggesting that binding of two (or possibly one) molecules of IP_3 is sufficient for channel opening. Interestingly, moderate concentrations of EGTA (approximately 25 μM) caused a much greater reduction in n_H than the same concentrations of BAPTA, further implying that inter-, rather than intra-cluster interactions are the main factor contributing to the high cooperativity under physiological conditions.

Potentiation of Ca^{2+} signalling by low [EGTA]

Ca^{2+} signals evoked by strong photorelease of IP_3 became progressively smaller with increasing concentrations of EGTA and BAPTA, as might be expected because the buffers will compete with the indicator dye for available Ca^{2+} as well as reducing Ca^{2+} liberation by impairing CICR. On the other hand, EGTA (but not BAPTA) actually potentiated responses evoked by weak photorelease of IP_3 by as much as 100 % (Fig. 3*C*). This surprising finding is consistent with a recent demonstration that slow, mobile Ca^{2+} buffers (parvalbumin and EGTA) promote puff activity in *Xenopus* oocytes, probably by sensitizing IP_3R to resting levels of IP_3 (John *et al.* 2001). Potentiation of Ca^{2+} excitability by expression of specific endogenous buffers may, therefore, play an important role in regulating cellular signalling. The underlying mechanism is unclear (John *et al.* 2001), but effects on cluster–cluster interactions are implicated because potentiation is most prominent with slow buffers, appears not to result from changes in resting free [Ca^{2+}], and does not correlate with binding of Ca^{2+}-free forms of different buffers to IP_3Rs (Richardson & Taylor, 1993; John *et al.* 2001).

Cluster–cluster interactions prolong Ca^{2+} liberation

Ca^{2+} signals during local Ca^{2+} puffs persist for only a few hundred milliseconds (Yao *et al.* 1995; Sun *et al.* 1998), whereas Ca^{2+} elevations during global waves decay over several seconds (e.g. Fig. 2). We originally thought that this difference might reflect differences in Ca^{2+} clearance, and that the kinetics of Ca^{2+} liberation were similar during these local and global events. Specifically, it seemed that Ca^{2+} liberated at a 'point' source (as during a puff) would rapidly dissipate by 3-dimensional diffuse into the vast volume of the oocyte, whereas the spatially extensive Ca^{2+} release during a wave would be cleared primarily by slower processes such as sequestration back into the e.r. (Yao *et al.* 1995). However, the experiment of Fig. 7 indicates that this is not a full explanation, because IP_3-evoked Ca^{2+} signals

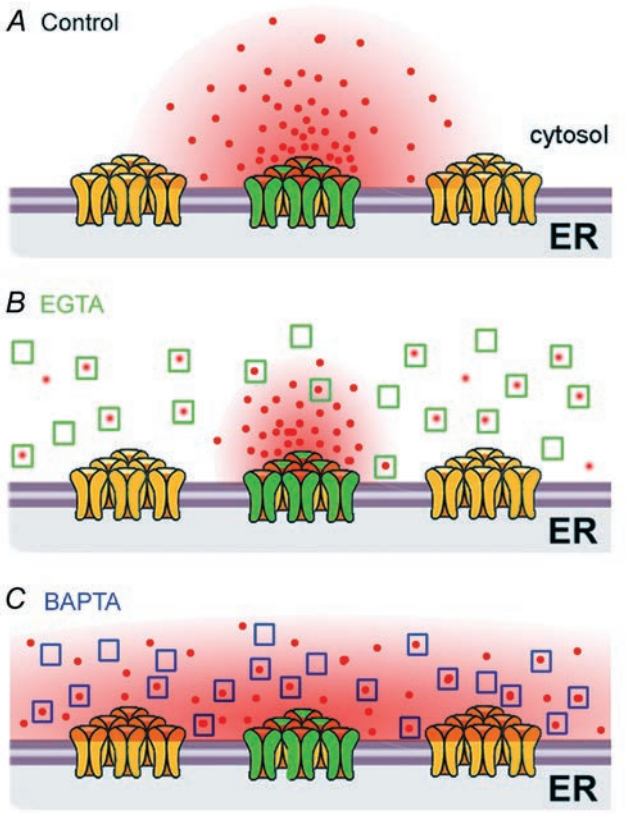

Figure 10. Cartoon illustrating the distribution of Ca^{2+} ions around IP_3R clusters, and how communication between IP_3Rs may be affected by mobile buffers with differing binding kinetics

A, without added buffer, Ca^{2+} ions liberated through open IP_3 at a cluster diffuse a few micrometres and, depending on [IP_3], may or may not trigger CICR at adjacent clusters. *B*, EGTA acts too slowly to disrupt Ca^{2+} diffusion and CICR within clusters, but binds Ca^{2+} ions as they diffuse between clusters and rapidly 'shuttles' them away, so as to disrupt cluster–cluster interactions. *C*, BAPTA binds Ca^{2+} ions sufficiently quickly to disrupt Ca^{2+} communication between IP_3Rs within individual clusters, whilst promoting Ca^{2+} communication between clusters by acting as a rapid Ca^{2+} shuttle.

decayed much more slowly than equivalent signals evoked by extracellular Ca^{2+} influx through voltage-gated channels. Instead, we conclude that IP_3-evoked waves are prolonged largely because Ca^{2+} efflux from the e.r. is biphasic. That is to say, a large, but rapidly terminating flux during the rising phase of the wave is followed by a 'tail' of Ca^{2+} efflux which, though small, is sufficiently prolonged that it greatly slows the decline of cytosolic $[Ca^{2+}]$ (Fig. 8*A*). The actions of EGTA and BAPTA on global Ca^{2+} signals to respectively speed and slow their decay can then be understood in terms of their relative effects on the fast and slow components of Ca^{2+} efflux. EGTA almost abolishes the slow component while having little effect on the fast component, whereas BAPTA selectively attenuates the fast component and prolongs the slow component (Fig. 8*B* and *C*).

Termination of Ca^{2+} flux through IP_3Rs thus appears to involve two distinct processes. Flux at individual clusters acting in isolation (at low $[IP_3]$, or after uncoupling with EGTA) ceases abruptly and stochastically within ~100 ms, and shows an 'adaptive' property such that it can be reactivated by further elevation of $[IP_3]$ (Callamaras & Parker, 2000). On the other hand, clusters recruited during a wave show an initial large Ca^{2+} efflux with a time course similar to that of puffs, and then abruptly transition to a state in which they continue to 'leak' Ca^{2+} at a low rate for several seconds. The mechanisms underlying this transition remain unknown, but the striking action of EGTA to attenuate the slow release suggests that it involves diffusional spread of Ca^{2+} between clusters, such that each continues to maintain others in an activated state. Moreover, the importance of the slow release component in shaping Ca^{2+} transients further emphasizes the role of buffers in cell signalling. Although the slow Ca^{2+} flux is small, its persistence means that the total amount of Ca^{2+} liberated is greater than that during the fast component; and attenuation of the slow component by EGTA shortens the duration of Ca^{2+} spikes as much as 10-fold.

Physiological roles of buffers in cellular Ca^{2+} signalling

Our results point to the importance of buffering kinetics in shaping the spatial and temporal patterning of Ca^{2+} signals generated by intracellular Ca^{2+} liberation through Ca^{2+}-sensitive release channels – effects that are more complex than for signals arising from a fixed 'pulse' of Ca^{2+}, as with Ca^{2+} entry through voltage-gated channels (e.g. Lee *et al.* 2000). For convenience we utilized the synthetic buffers EGTA and BAPTA, which are not normally present within cells. However, preliminary experiments with endogenous mobile Ca^{2+}-binding proteins (Dargan *et al.* 2003) point out the physiological relevance of our results. In particular, parvalbumin – a mobile Ca^{2+} buffer with slow Ca^{2+} binding kinetics (Lee *et al.* 2000*b*; Schmidt *et al.* 2003) – balkanized Ca^{2+} signals and accelerated their decay similar to EGTA; whereas the fast buffer calretinin (Edmonds *et al.* 2000) produced BAPTA-like effects. Although there are obvious differences between small-molecule and protein buffers (such as differing mobility and possibility of protein–protein interactions), the emergent theme is that the kinetics of a buffer are the key parameters defining its actions in shaping IP_3-mediated Ca^{2+} signals. Moreover, this theme is likely to extend to mammalian systems because the clustered distribution of IP_3Rs in the *Xenopus* oocyte is mirrored in diverse mammalian cells (Bootman *et al.* 1997; Simpson *et al.* 1997). We finally note that ryanodine receptors (RyRs), the other major class of intracellular Ca^{2+} release channel, also communicate via CICR (Berridge, 1997), so that their signalling may similarly be susceptible to shaping by mobile Ca^{2+} buffers.

REFERENCES

Allbritton NL, Meyer T & Stryer L (1992). Range of messenger action of calcium ion and inositol 1,4,5-trisphosphate. *Science* **258**, 1812–1815.

Andressen C, Blumcke I & Celio MR (1993). Calcium-binding proteins: selective markers of nerve cells. *Cell Tissue Res* **271**, 181–208.

Berridge MJ (1997). Elementary and global aspects of calcium signalling. *J Physiol* **499**, 291–306.

Berridge MJ, Lipp P & Bootman MD (2000). The versatility and universality of calcium signalling. *Nat Rev Mol Cell Biol* **1**, 11–21.

Bezprozvanny I, Watras J & Ehrlich BE (1991). Bell-shaped calcium-response curves of $Ins(1,4,5)P_3$- and calcium-gated channels from endoplasmic reticulum of cerebellum. *Nature* **351**, 751–754.

Bootman M, Niggli E, Berridge M & Lipp P (1997). Imaging the hierarchical Ca^{2+} signalling system in HeLa cells. *J Physiol* **499**, 307–314.

Callamaras N, Marchant JS, Sun XP & Parker I (1998*a*). Activation and co-ordination of InsP3-mediated elementary Ca^{2+} events during global Ca^{2+} signals in *Xenopus* oocytes. *J Physiol* **509**, 81–91.

Callamaras N & Parker I (1998). Caged inositol 1,4,5-trisphosphate for studying release of Ca^{2+} from intracellular stores. *Methods Enzymol* **291**, 380–403.

Callamaras N & Parker I (1999). Radial localization of inositol 1,4,5-trisphosphate-sensitive Ca^{2+} release sites in *Xenopus* oocytes resolved by axial confocal linescan imaging. *J Gen Physiol* **113**, 199–213.

Callamaras N & Parker I (2000). Phasic characteristic of elementary Ca^{2+} release sites underlies quantal responses to IP_3. *EMBO J* **19**, 3608–3617.

Callamaras N, Sun XP, Ivorra I & Parker I (1998*b*). Hemispheric asymmetry of macroscopic and elementary calcium signals mediated by $InsP_3$ in *Xenopus* oocytes. *J Physiol* **511**, 395–405.

Dargan SL, Demuro A, Marchant J, Callamaras N, Schwaller B & Parker I (2003). Shaping of IP3-mediated Ca^{2+} signals by Ca^{2+} buffers and Ca^{2+} binding proteins. *Biophys J* **84**, suppl., 384a.

Dawson SP, Keizer J & Pearson JE (1999). Fire-diffuse-fire model of dynamics of intracellular calcium waves. *Proc Natl Acad Sci U S A* **96**, 6060–6063.

Edmonds B, Reyes R, Schwaller B & Roberts WM (2000). Calretinin modifies presynaptic calcium signaling in frog saccular hair cells. *Nat Neurosci* **3**, 786–790.

Falcke M (2003). Buffers and oscillations in intracellular Ca^{2+} dynamics. *Biophys J* **84**, 28–41.

Finch EA, Turner TJ & Goldin SM (1991). Calcium as a coagonist of inositol 1,4,5-trisphosphate-induced calcium release. *Science* **252**, 443–446.

Hirota J, Michikawa T, Miyawaki A, Furuichi T, Okura I & Mikoshiba K (1995). Kinetics of calcium release by immunoaffinity-purified inositol 1,4,5-trisphosphate receptor in reconstituted lipid vesicles. *J Biol Chem* **270**, 19046–19051.

Horne JH & Meyer T (1997). Elementary calcium-release units induced by inositol trisphosphate. *Science* **276**, 1690–1693.

Iino M (1990). Biphasic Ca^{2+} dependence of inositol 1,4,5-trisphosphate-induced Ca^{2+} release in smooth muscle cells of the guinea pig taenia caeci. *J Gen Physiol* **95**, 1103–1122.

John LM, Mosquera-Caro M, Camacho P & Lechleiter JD (2001). Control of IP_3-mediated Ca^{2+} puffs in *Xenopus laevis* oocytes by the Ca^{2+}-binding protein parvalbumin. *J Physiol* **535**, 3–16.

Kidd JF, Fogarty KE, Tuft RA & Thorn P (1999). The role of Ca^{2+} feedback in shaping $InsP_3$-evoked Ca^{2+} signals in mouse pancreatic acinar cells. *J Physiol* **520**, 187–201.

Lechleiter JD & Clapham DE (1992). Molecular mechanisms of intracellular calcium excitability in *X. laevis* oocytes. *Cell* **69**, 283–294.

Lee SH, Rosenmund C, Schwaller B & Neher E (2000*a*). Differences in Ca^{2+} buffering properties between excitatory and inhibitory hippocampal neurons from the rat. *J Physiol* **525**, 405–418.

Lee SH, Schwaller B & Neher E (2000*b*). Kinetics of Ca^{2+} binding to parvalbumin in bovine chromaffin cells: implications for $[Ca^{2+}]$ transients of neuronal dendrites. *J Physiol* **525**, 419–432.

Lin Z, Haus S, Edgerton J & Lipscombe D (1997). Identification of functionally distinct isoforms of the N-type Ca^{2+} channel in rat sympathetic ganglia and brain. *Neuron* **18**, 153–166.

Mak DO, McBride S & Foskett JK (1998). Inositol 1,4,5-trisphosphate activation of inositol trisphosphate receptor Ca^{2+} channel by ligand tuning of Ca^{2+} inhibition. *Proc Natl Acad Sci U S A* **95**, 15821–15825.

Marchant JS & Parker I (2000). Functional interactions in Ca^{2+} signaling over different time and distance scales. *J Gen Physiol* **116**, 691–696.

Marchant JS & Taylor CW (1997). Cooperative activation of IP_3 receptors by sequential binding of IP_3 and Ca^{2+} safeguards against spontaneous activity. *Curr Biol* **7**, 510–518.

Meyer T, Wensel T & Stryer L (1990). Kinetics of calcium channel opening by inositol 1,4,5-trisphosphate. *Biochemistry* **29**, 32–37.

Morris SA, Correa V, Cardy TJ, O'Beirne G & Taylor CW (1999). Interactions between inositol trisphosphate receptors and fluorescent Ca^{2+} indicators. *Cell Calcium* **25**, 137–142.

Nagerl UV, Novo D, Mody I & Vergara JL (2000). Binding kinetics of calbindin-D(28k) determined by flash photolysis of caged Ca^{2+}. *Biophys J* **79**, 3009–3018.

Naraghi M (1997). T-jump study of calcium binding kinetics of calcium chelators. *Cell Calcium* **22**, 255–268.

Neher E (2000). Calcium buffers in flash-light. *Biophys J* **79**, 2783–2784.

Parker I, Callamaras N & Wier WG (1997). A high-resolution, confocal laser-scanning microscope and flash photolysis system for physiological studies. *Cell Calcium* **21**, 441–452.

Parker I, Yao Y & Ilyin V (1996). Fast kinetics of calcium liberation induced in *Xenopus* oocytes by photoreleased inositol trisphosphate. *Biophys J* **70**, 222–237.

Parys JB, Sernett SW, Delisle S, Snyder PM, Welsh MJ & Campbell KP (1992). Isolation, characterization, and localization of the inositol 1,4,5-trisphosphate receptor protein in *Xenopus laevis* oocytes. *J Biol Chem* **267**, 18776–18782.

Richardson A & Taylor CW (1993). Effects of Ca^{2+} chelators on purified inositol 1,4,5-trisphosphate ($InsP_3$) receptors and $InsP_3$-stimulated Ca^{2+} mobilization. *J Biol Chem* **268**, 11528–11533.

Roberts WM (1994). Localization of calcium signals by a mobile calcium buffer in frog saccular hair cells. *J Neurosci* **14**, 3246–3262.

Schmidt H, Brown EB, Schwaller B & Eilers J (2003). Diffusional mobility of parvalbumin in spiny dendrites of cerebellar purkinje neurons quantified by fluorescence recovery after photobleaching. *Biophys J* **84**, 2599–2608.

Schwaller B, Meyer M & Schiffmann S (2002). 'New' functions for 'old' proteins: The role of the Ca^{2+} binding proteins calbindin D-28K, calretinin and parvalbumin in cerebellar physiology. Studies with knockout mice. *Cerebellum* **1**, 241–258.

Shuai JW & Jung P (2002). Stochastic properties of Ca^{2+} release of inositol 1,4,5-trisphosphate receptor clusters. *Biophys J* **83**, 87–97.

Shuai JW & Jung P (2003). Optimal ion channel clustering for intracellular calcium signaling. *Proc Natl Acad Sci U S A* **100**, 506–510.

Simpson PB, Mehotra S, Lange GD & Russell JT (1997). High density distribution of endoplasmic reticulum proteins and mitochondria at specialized Ca^{2+} release sites in oligodendrocyte processes. *J Biol Chem* **272**, 22654–22661.

Song LS, Sham JS, Stern MD, Lakatta EG & Cheng H (1998). Direct measurement of SR release flux by tracking 'Ca^{2+} spikes' in rat cardiac myocytes. *J Physiol* **512**, 677–691.

Stern MD (1992). Buffering of calcium in the vicinity of a channel pore. *Cell Calcium* **13**, 183–192.

Sun XP, Callamaras N, Marchant JS & Parker I (1998). A continuum of $InsP_3$-mediated elementary Ca^{2+} signalling events in *Xenopus* oocytes. *J Physiol* **509**, 67–80.

Swillens S, Dupont G, Combettes L & Champeil P (1999). From calcium blips to calcium puffs: theoretical analysis of the requirements for interchannel communication. *Proc Natl Acad Sci U S A* **96**, 13750–13755.

Tsien RY (1980). New calcium indicators and buffers with high selectivity against magnesium and protons: design, synthesis, and properties of prototype structures. *Biochemistry* **19**, 2396–2404.

Yao Y, Choi J & Parker I (1995). Quantal puffs of intracellular Ca^{2+} evoked by inositol trisphosphate in *Xenopus* oocytes. *J Physiol* **482**, 533–553.

Acknowledgements

Plasmids containing cDNA clones coding for the N-type Ca^{2+} channel α_{1B-d} and β_3 subunits were a kind gift from Diane Lipscombe. We thank Dr Angelo Demuro for *in vitro* transcription, expressing N-type Ca^{2+} channels in oocytes, and helping with experiments of Fig. 7; and Dr Brian Edmonds for helpful discussion. Funded by NIH grants GM48071 and GM58329.